X-622-67-352

NASA TM X-55893

PRELIMINARY RESULTS FROM AIRCRAFT FLIGHT TESTS OF AN ELECTRICALLY SCANNING MICROWAVE RADIOMETER

C. CATOE
W. NORDBERG
P. THADDEUS
G. LING

AUGUST 1967

GODDARD SPACE FLIGHT CENTER
GREENBELT, MARYLAND

X-622-67-352

PRELIMINARY RESULTS FROM AIRCRAFT FLIGHTS OF AN ELECTRICALLY SCANNING MICROWAVE RADIOMETER

C. Catoe
W. Nordberg
P. Thaddeus
G. Ling

August 1967

GODDARD SPACE FLIGHT CENTER
Greenbelt, Maryland

BLANK PAGE

PRELIMINARY RESULTS FROM AIRCRAFT FLIGHTS OF AN ELECTRICALLY SCANNING MICROWAVE RADIOMETER

C. Catoe
W. Nordberg
P. Thaddeus
G. Ling

ABSTRACT

The Electrically Scanning Microwave Radiometer, which was flown on NASA's Convair 990 aircraft proved the feasibility of extending the spectral range of meteorological satellite radiation measurements from the infrared regions to much longer microwave wavelengths (1.55 cm). The radiometer consists of a microwave receiver and a two dimensional, 18 x 18 inch, phased-array antenna. The phased array antenna was designed to scan a beam, 2.7 degrees wide, electrically through an angle of ±50° from nadir. The direction of beam scan is perpendicular to the direction of the aircraft motion so that two dimentional maps of the earth's brightness temperature are made.

Flights were conducted over Arctic Ocean ice, Alaskan tundra and snow, Southwestern U. S. deserts, Eastern and Mid-west U. S. farmland, Yucatan tropical forests, and storms and rain clouds over land and water. Data have not been completely reduced; however, preliminary indications from qualitative, real time displays (facsimile printer), over selected areas, demonstrate that this radiometer performed as expected.

Indications are that mapping was achieved with the desired spatial resolution (2.7° beamwidth), and with useful radiometric accuracy. Land-water and ice contrasts were mapped with outstanding clarity in clear atmosphere as well as under all conditions of cloudiness, and rain clouds and storm activity over oceans could be positively identified even, and especially, when other cloudiness obscured such identification visually or by infrared techniques. The aircraft tests proved that scanning microwave radiometry will be an extremely useful sensor for mapping areas of heavy rainfall and the extent and thickness of sea ice ultimately from spacecrafts in orbit, and independent of cloud conditions.

CONTENTS

BLANK PAGE

PRELIMINARY RESULTS FROM AIRCRAFT FLIGHTS OF AN ELECTRICALLY SCANNING MICROWAVE RADIOMETER

I. INTRODUCTION

During the period from 5 May to 7 June, 1967, observations of the Earth over a wide geographical area were made with an imaging microwave radiometer (radiotelescope) aboard the NASA Convair 990. The radiometer operated at a frequency of 19.35 GHz ($\lambda = 1.55$ cm), and was electrically scanned over an angle of $\pm 50^{\circ}$ with respect to the nadir. A total of fourteen flights were made which extended as far north as Point Barrow, Alaska, and as far south as the Yucatan peninsula. Several flights covered selected areas in the western and southwestern United States and the adjacent Pacific Ocean; two transcontinental flights surveyed a strip of the southern, central, and eastern United States.

Microwave radiometric observations of the earth have only been made episodically in the past, usually over limited areas, and seldom with a scanning instrument. The radiometer used in the work reported here was designed to make the first global microwave studies of the earth from a meteorological satellite. It is extremely lightweight, rugged, and low in power consumption, representing what we have designated an "aircraft prototype" of the satellite flight models, and conforming very closely to the flight models in its overall specifications.

The purpose of the aircraft flights described here was twofold: (1) to confirm and extend the laboratory and range calibration of the instrument, particularly under field conditions and in companion with the infrared sensors on board the aircraft, and (2) to study as wide a variety of atmospheric and terrain features as possible in order to demonstrate the meteorological and geophysical utility of the instrument.

II. THE ELECTRICALLY SCANNING MICROWAVE RADIOMETER

The electrically scanning microwave radiometer was built under contract to the Goddard Space Flight Center by the Space General Corporation, El Monte, California and is described in detail in a Space General report (1). Its basic components are a microwave superheterodyne receiver, a two-dimensional phased array antenna, and a beam steering computer. Figure 1 shows the 18" x 18" x 6" antenna and the

8" x 6" x 13" module which contains the receiver and beam steering computer. The nitrogen dewar also shown in Figure 1 is required on the aircraft flight model in order to furnish a cold reference blackbody. It will be replaced on the spacecraft version of the instrument by a small horn which views cold space. The antenna weight is eight pounds, and the receiver and computer together weigh about twelve pounds. All circuitry is solid state, with approximate power consumption of 14.8 watts.

The receiver and phased array operate at a frequency of 19.35 GHz (wavelength of 1.55 cm) over a bandwidth of 400 MHz. This exact frequency was chosen to coincide with one of the radio astronomy channels adopted at the 1963 Extraordinary Radio Conference at Geneva in order to avoid interference by ground-based radar, although the radiometer bandwidth is twice that of the reserved channel. The phased array consists of 49 linear arrays, whose relative phase is controlled by small ferrite phase shifters located at the input of each of the linear arrays. A small computer increments the currents through each of the phase shifters in such a way as to cause the beam of the two-dimensional array to scan incrementally in a saw-tooth mode through an angle of ±50° with respect to the normal to the array, and in the plane perpendicular to the linear arrays. On the aircraft or spacecraft, the antenna is aligned with the individual arrays pointing in the direction of motion of the vehicle, so that the scan is perpendicular to the direction of motion, and a thermal image of the earth is built up scan-by-scan as the vehicle advances. The sense of polarization received is such that the electric vector is always parallel to the earth's surface. The width of the main beam at the 3 db points varies slightly with scan from 2.7° broadside to 3.0° at ±50°.

The Dicke-type superheterodyne receiver uses a ferrite switch to compare the antenna signal to the thermal emission from a matched hot load at a switching frequency of 600 Hz. The hot load is located in a regulated oven at 338°K. At intervals between scans, the 77°K cold load replaces the antenna beam input to the receiver for the purpose of calibration. The gain of the receiver is adjusted so that the output can be read in about 500 linear steps over the temperature range between the hot load and the cold load. A logics circuit produces this output in digital form. The radiometer can thus measure radiances corresponding to temperatures between about 100°K and 330°K with an accuracy of about 2°K.

III. AIRCRAFT INSTALLATION OF THE RADIOMETER

A simplified block diagram of the functioning of the radiometer system on the aircraft is shown in Figure 2. It consists of antenna and

radome, radiometer receiver, interface equipment, facsimile recorder, incremental digital tape recorder, and cryogenic flask.

The antenna/radome assembly and radiometer receiver are mounted on opposite sides of a specially designed access door located (between station 1040 to 1097) in the bay of the Convair 990 aircraft. A separate aerodynamic fairing is attached to the fuselage of the aircraft to serve as an aerodynamic buffer for the antenna which projects below the aircraft. A radome which consists of a 0.95 cm sheet of Rexolite is placed below the flat phased array surface in order not to expose the antenna to aerodynamic effects, moisture, dust, or other foreign matter. High purity dry nitrogen is fed into the antenna under positive pressure to prevent moisture buildup. The nitrogen gas introduced into the antenna is bled off at a controlled rate to the surrounding atmosphere.

On the aircraft, a cryogenically cooled load is used as a temperature reference in place of a space viewing reference horn to be used on the spacecraft. The cold reference consists of a waveguide connected to a copper heat sink which is cooled to the temperature of the cryoflask filled with liquid nitrogen at a temperature of 77°K.

The radiometer is designed to operate ultimately from an earth oriented spacecraft at an orbital altitude of about 1000 km. For that application, the scan rate of the antenna beam was originally designed for about one scan per six seconds to provide contiguous mapping of the Earth since the spacecraft would take about six seconds to travel the distance subtended by the antenna beam on the surface of the Earth (40 km). On the aircraft, this distance is considerably reduced (400 m for a flight level of 10 km and 40 for 1 km). Thus, the aircraft covers the distance subtended by the antenna beam in a much shorter time (about 2 seconds at 10 km and about 1 second at 2 km). Therefore, two frequency multiplier circuits are incorporated in the interface equipment to increase the scan rate for the aircraft flights. Two scan rates can be selected manually: For high level flights, scan rates are set at one scan per two seconds, for lower level flights (below 3 km) at one scan per seconds. Thus, scanning at 50° on each side of the aircraft produces contiguous maps of radiance covering a strip about 23.8 km wide from an altitude of 10 km and about 7.2 km wide from an altitude of about 3 km.

The radiometric output is recorded digitally on tape in a form suitable for direct entry into a digital computer. Calibration data such as, for example, temperatures of the various reference loads are also

recorded on this tape at regular intervals. The relatively low data rate allows the use of an inexpensive incremental digital tape transport on board the aircraft to record the data in a computer compatible form. The incremental digital tape transport advances one tape character at a time, and there is no requirement to advance the tape at a constant rate to provide proper character pack for the computer input operation; this feature allows for insertion of the various required housekeeping and auxiliary functions in essentially a non-synchronized manner. Recorded also are timing signals provided by a separate time code generator, synchronized with a universal time standard (WWV).

The radiometer output and time signals are also fed into a facsimile printer. The printer is utilized to provide immediate display of the area scanned to facilitate the on-board correlation of data. The facsimile printer provides a gray scale display in which high intensity radiation (warm temperatures) is rendered dark and low intensity (cold temperatures) corresponds to light shades. The few gray shades discernible on the facsimile prints, of course, permit only qualitative, but real time, data analysis while the digital recordings contain the high accuracy information necessary for quantitative analysis.

In addition, photographic images of the observed terrain are recorded on a separate tape recorder from a TV camera and on black and white and color film from various aerial cameras. The TV tape recorder also has an audio track available on which time code, general description of observed areas, and general meteorological conditions can be superimposed to facilitate correlation and analysis of data. Additional experiments on the aircraft provide supporting observations with infrared spectrometers and radiometers.

IV. RESULTS

The preliminary analysis presented here based primarily on spot checks of the qualitative facsimile recordings, was intended to verify the potential of meteorological observations from a satellite in this portion of the spectrum with this instrument. The essential features of such observations were pointed out by Thaddeus in a proposal to fly this instrument on a Nimbus satellite (2):

(a) to detect cells of heavy precipitation over oceans and to distinguish such cells by virtue of their greater brightness temperatures from other, less active, cloud masses which would be nearly transparent at this wavelength. The ocean surface

which is highly reflecting (reflectivity ≈ 0.6) in the microwave range would provide a uniform background of extremely low brightness temperature. This was first suggested by Buettner (3) as a method to detect precipitation over water.

(b) To measure the brightness temperature of the solid surface of the earth, even in the presence of moderately thick, non precipitating clouds. Depending on additional knowledge of the characteristics of these surfaces certain inferences could be made. Over vegetation, the emissivity is expected to be very high (greater than 0.9) and the true surface temperature could be inferred; over dry, barren soil the emissivity would be somewhat lower and over moist areas emissivity would decrease further with moisture content and, in this case, lower brightness temperatures would correspond to very moist, or flooded regions.

(c) To measure the contrast between water and ice, and possibly the thickness of the ice in polar regions, even in the presence of clouds. Since ice has a very large transmissivity it would have to be very thick to produce a brightness temperature which would be an accurate measure of its physical temperature. Thinner ice would be partially transparent allowing the cold sky to be reflected from the underlying water, resulting in lower brightness temperatures as the ice became thinner. As there are very few heavy rain clouds in polar regions, these observations would be unaffected by cloudiness.

The examples resulting from our aircraft flights, which are discussed below, will demonstrate that these expectations were generally fulfilled and that this radiometer is excellently suited to perform such observations from a satellite.

A. Ocean Background and Precipitation

Of the fourteen flights conducted during the period 5 May to 7 June 1967, twelve covered major bodies of water. Six flights were almost entirely over water. Observations were made over: the Pacific Ocean, off the Coasts of California and Oregon, and between Alaska and California; the Gulf of Mexico; the Arctic Ocean; the Atlantic Ocean; Chesapeake Bay; and many rivers and lakes. In all cases investigated so far, the observed brightness temperatures of water were uniquely low. They ranged from about 110°K over the Arctic Ocean to about 140°K over the Gulf of Mexico. We believe that the higher temperatures at

low latitudes are primarily due to some emission by atmospheric water vapor with the difference in water temperature playing only a secondary role. Over water, low brightness temperatures were observed regardless of cloud condition, provided that the clouds did not contain large water drops of heavy rain. High altitude cirrus layers of 2000 - 3000 feet thickness and low altitude stratus layers up to 10,000 feet thick over the North Pacific were verified to have little effect on the observed low brightness temperatures (about 120° K) of the water.

On the other hand, towering cumulus clouds containing cells of heavy rainfall were overflown and penetrated over the Gulf of Mexico, about 200 miles southeast of New Orleans (Figure 3a). Bases of these clouds were near 2000 feet and tops between 25,000 and 35,000 feet. The strongest rain cells verified by the aircraft weather radar and by visual observations (left side of Figure 3a), produced an increase in brightness temperature of about 120° K. Clouds containing less rainfall with lower altitude tops (center of Figure 3a) produced a lesser increase in brightness temperatures, and the wind blown tops (upper right Figure 3a) consisting of thick cirrus, which visually appeared indistinguishable from the rain clouds when seen from the top, showed practically no increase. Figure 3b shows a composite of aerial photographs taken during an over flight of the cloud mass shown in Figure 3a from left to center at about 36,000 feet. The numbers shown across the bottom, center and top of the photograph represent the digital output of the microwave radiometer and correspond (after appropriate correction for calibration) to the measured brightness temperatures over corresponding areas of the photograph. A calibration correction of about -20° K must be applied to each number to obtain the correct brightness temperature. It can be seen that the cloud at the bottom of Figure 3b (at 14:46:03GMT) shows the same brightness temperature range as the clear ocean in the center (14:47:05 GMT), namely 135 to 140° K. The same situation exists in Figure 3c where the aerial photograph shows an extremely uniform, dense cloud. The aircraft position at 14:53:31 GMT (center Figure 3c) was at 38,000 ft. over the cirrus anvil shown at right in Figure 3a. We verified that these clouds, although quite thick, were not raining at that time. The cloud overflown at 14:48:49 GMT (top of Figure 3b), however, contained heavy precipitation. It corresponds to the buildups seen at left in Figure 3a. Here the brightness temperatures range as high as 257° K. This corresponds to an increase of 122° K over the clear ocean background or over the other, nonprecipitating clouds. This observation confirms the perhaps most powerful potential of scanning microwave radiometer for meteorological satellites: the distinction of rainclouds from other clouds, which cannot be made with existing satellite instruments in the visual and infrared.

B. Land and Water Observations over Clouds.

The most striking contrasts in brightness temperature over continents are observed between lakes, rivers, inundated regions on one hand and drier land and vegetation on the other. Aside from liquid water surfaces, all areas overflown and analyzed so far displayed brightness temperatures which were commensurate with relatively high emissivity values (varying above 0.9). There were variations in brightness temperature over many areas, especially over farmland, however, these variations were almost one order of magnitude smaller than those observed between land and water. A quantitative analysis of all the data is necessary to separate actual temperature variations of the surface from emissivity variations and to, possibly, ascribe certain changes in the surface morphology to these emissivity variations.

A good example of land and water contrast is shown in Figure 4a. It shows a facsimile recording for a period of about one minute while the aircraft was passing over the Ohio river at 37,300 ft. between Evansville, Illinois and Louisville, Kentucky. Dark shades correspond to warm, and light shades to cold, brightness temperatures. For comparison, a simultaneous aerial photograph over the same area is shown in Figure 4b. Because the 74° field of view of the aerial camera is less than the radiometer's scan width, which is 100 degrees, the facsimile display covers a somewhat wider strip than the aerial photograph. The facsimile record displays a drastic contrast between the river and the surrounding farmland and forests. A check of digitally recorded brightness temperatures shows a difference of over 100°K. Lesser variations appear over the land itself. The looping, and now cutoff, old river bed which appears in the center of the photograph can be recognized by a corresponding colder (whiter) loop in the facsimile display. This brightness temperature difference could be due to water remaining in the old river bed. However, the photograph gives no indication of water, except for a very few scattered puddles and pools. Rather, we speculate that the contrast is caused by the difference in terrain: cultivated fields in the old river bed and forrested hills surrounding it. The fact that somewhat colder temperatures in the right center, and across the river in the lower right, correspond to farmed areas in the photograph, suggests that the lower temperatures are due to lower emissivity of farmland compared to forests.

Figures 5a, b and c illustrate that similar contrasts can be observed through a complete overcast. Figure 5a is the aerial photograph of a stratus cloud deck extending from near the ground up to about 6,000 feet. The position of the aircraft was over St. Louis, Mo., at an altitude of 37,300 feet. Figure 5b shows the corresponding facsimile display of

brightness temperatures. The river system consisting of the Mississippi (top and left), the Illinois (branching off on the left), and the Missouri (center), is shown in the corresponding topographic map (Figure 5c). A very cold (light) area is seen in the lower center. This may correspond to swampy and flooded regions. Lesser contrast can probably again be interpreted as vegetation differences, such as farmlands in the upper right, north of the Missouri River, and denser vegetation between the Missouri and Mississippi Rivers.

A five minute strip of a facsimile display obtained from 33,000 feet during a pass from the western foothills of the Sierra Nevada to Mono Lake, California is shown in Figure 6a. Two bodies of water stand out: Mono Lake at the top and the Hetch Hetchy Reservoir at the bottom. The cold area in the center corresponds to the Sierra Nevada Mountain range, which was snow covered with elevations ranging up to 12,600 feet. Brightness temperatures varied by more than 30°C between the snow covered mountain tops and the plateau around Mono Lake. An island can be seen in Mono Lake and warmer temperatures on the east side of the Sierra indicate two valleys descending toward Mono Lake. A topographic map for the same area is shown in Figure 6b.

C. Sea, Ice and Snow Observations.

Most interesting contrasts were obtained over the Arctic tundra, near Pt. Barrow, Alaska. Figure 7 shows a facsimile display obtained during a pass at 35,000 ft. outbound over the tundra, over the coast near Pt. Barrow, over the open Arctic Ocean and finally over pack ice of increasing solidity, along a course indicated on the Map (Figure 8). Figure 9 shows the facsimile display obtained inbound over the same path, but at much lower altitudes. The aircraft was descending from 35,000 ft. about 100 miles off shore to less than 500 feet over Pt. Barrow. It can be seen that the features in Figure 9 correspond to the features seen along a narrow center strip of Figure 7, allowing for perspective distortion due to the much lower altitude of the aircraft and reversing left and right due to the opposite direction of flight.

There are six consistent features to be noted in the brightness temperature patterns:

(1) Relatively uniform temperatures were mapped over solid pack ice after 00:32 GMT on the outbound pass and before 00:56 GMT on the inbound pass. A stratus cloud deck covered the entire area north of 71°N and extended from a height of about 800 feet to about 2,500 feet. All observations prior to 00:58 GMT were made from

above this cloud deck and photographs show only the cloud cover. Microwave brightness temperatures were not noticeably influenced by the cloud cover. Where the ice was verified as solid, brightness temperatures were about 245°K. This is about 20°C lower than the ice surface temperatures measured by the infrared radiometer, which corresponds to an emissivity of 0.90 - 0.95 for the ice surface. This indicates that the ice thickness was sufficient not to permit penetration of microwave radiation from the water below. Drillings which were made in this area two weeks prior to our observations, determined that the ice thickness was about 1 - 2 meters (4).

(2) Thin and broken ice was observed between 00:28 GMT and 00:32 GMT outbound and between 00:56 GMT and 01:01:30 GMT inbound. A photograph of this ice condition is shown in Figure 10. This was obtained on the inbound pass from an altitude of about 500 feet after the aircraft had penetrated the stratus cloud deck. As the ice became very thin in this area the brightness temperatures decreased sharply. Many cracks revealing open water at brightness temperature of about 130°K lower than over the ice can be seen between the ice, both inbound and outbound. One very large crack about 2 km wide was seen on the inbound pass between 00:53 GMT and 00:54 GMT.

(3) A wide band of open water extends between 00:26:45 GMT and 00:28 GMT on the outbound between 01:01:35 GMT and 01:04 GMT on the inbound pass. Since the speed of the aircraft inbound at low altitude was only about one half the speed outbound at high altitude (about 230 m/sec.), it took twice the time to cover the distance of the band of open water, about 17 km, on the inbound pass. During the outbound pass the open water could be observed only with the microwave radiometer. During the inbound pass, which was made below the cloud deck, visual and photographic verification of the open water was obtained. Brightness temperatures of about 110°K were measured with the microwave radiometer. Water temperature, inferred from infrared radiometer measurements, was about 271°K.

(4) A narrow strip of solid land and of massive ice build up along the shore of the Arctic Ocean was observed outbound near 00:26:40 GMT and inbound between 01:04:00 GMT and 01:04:39 GMT. This corresponds to a width of about 4 km. Brightness temperatures over the slightly snow covered land there were about the same or up to 10°C lower than over the Arctic Ocean ice. Temperatures

derived from the infrared radiometer were about 272°K. On the outbound pass, the radiometer covered a much wider area, because of the greater height. Relatively high temperatures were observed to the right of the aircraft between 00:25 GMT and 00:26 GMT. This area corresponds to the ice over Elson Lagoon to the east of Point Barrow (Figure 8). The surprising observations that the land to the southwest (left of aircraft) showed much lower brightness temperatures will be discussed below.

(5) Both passes, outbound and inbound, showed land areas where brightness temperatures were 15° - 20° C lower than those typical of thick ice or land, but still higher than those of water. This occurred between 00:23:20 GMT and 00:26:20 GMT outbound, and between 01:04:50 GMT and 01:09:50 GMT inbound. A feature of warmer temperatures typical of land or thick ice appeared as an "island" on the outbound pass near 00:24 GMT and could be seen again near 01:08:40 GMT to the left of the aircraft. The area of low brightness temperatures extended over a distance of about 40 km along which the photographs (Figure 11) showed a uniform snow-cover. Topographically this area is marshy tundra land. Further south (after 01:10 GMT) the snow cover is considerably less. A full explanation for this drastic brightness temperature contrast over so large an area will not be available before a complete reduction of the quantitative data. However, we speculate that these very low temperatures were caused by a layer of liquid water which, perhaps, lay beneath the melting snow cover. The snow layer covering the water must have been partially transparent and partially emitting at this wavelength. There was no water on top of the snow. Surface temperatures measured in the infrared over this area were about 268°K and show no variation between this area and the solid land overflown at 01:04 GMT and after 01:10 GMT inbound.

(6) Microwave brightness temperatures equal to those seen over the Arctic Ocean ice and those over the coast near Point Barrow were observed over the tundra more than 40 km inland (before 00:23:10 GMT outbound and after 01:10 GMT inbound). Although there is considerable non uniformity in the temperature, the warmer regions correspond to solid ground either bare or snowblown at radiances very consistent with an emissivity of 0.9 compared with surface temperatures measured in the infrared. The patches of lower radiance occasionally as low as that for water, correspond to a multitude of partially frozen, partially melted, lakes and rivers (Figure 12). The photograph (Figure 12) was taken about

50 km southeast of Point Barrow, Alaska, looking northward. The contrast in the terrain between bare land with frozen lakes to the south and more uniform snowcover to the north can be clearly seen. This contrast corresponds to the 15° - 20°C brightness temperature contrast observed by the microwave radiometer (near 1:10 GMT on the inbound facsimile display, Figure 9) with the colder area being to the north.

D. Other Noteworthy Brightness Temperature Observations

Other than between land and water, the strongest variations in brightness temperature were observed over farmland, especially of the Midwestern U. S. Comparisons with aerial photographs show that regions of lower brightness temperature generally correspond to areas free of vegetation while areas of more intense microwave emission correspond to more densely vegetated regions. One such example was already shown in Figure 4a. Another example of particularly great contrast is seen in Figure 13. This facsimile record was obtained from 37,300 ft. over Southern Indiana about 2 miles north of Evansville, heading east. Except for one dark (high brightness temperature) streak across the record, the entire lower portion of the facsimile display shows very low brightness temperatures. The upper half shows much higher brightness temperatures (darker shades) except for two spots in the center. The accompanying aerial photograph (Figure 14) shows that the eastern part of the facsimile record (lower portion) consisted mainly of fields devoid of vegetation. In the upper part most fields are covered by vegetation and, in part, by forests. One large spot of barren land, apparently a strip mine can be seen near the upper center of the picture. This corresponds to the spot of low brightness temperature around 23:22:10 GMT in the center of the facsimile display. The very low brightness temperature near 23:23:10 GMT at the center of the upper edge of the facsimile record corresponds to the small reservoir seen at the top of the picture. A cursory quantitative analysis of the digitally recorded data indicated a difference of about 15° to 20° C in the observed brightness temperatures between the upper and lower part of the facsimile display. Such brightness temperature gradients must be due to emissivity variations since infrared observations over the same area show that the surface temperatures varied by no more than 5°C between the vegetated regions and barren fields. Over the fields infrared temperatures were about 289°K. Over vegetation they were about 294°K. On that basis the emissivity of the vegetation would have been very close to 1.0 in the microwave region while the fields would have had an emissivity of about 0.95.

Another situation where the microwave radiometer indicated a marked drop in brightness temperatures was when the earth's surface was viewed at oblique angles, greater than 50° from the nadir. Since the scan is ±50° from the nadir when the aircraft is in level flight this brightness temperature decrease was observed only when the aircraft was banking. Figure 15 shows the facsimile record obtained during a 20° bank over the uniform ice pack of the Arctic Ocean. The aricraft was banking to the left and a brightness temperature difference of about 30°C was noted between the right and the left horizon starting at nadir angles of about 55°. Since banking angles never exceeded 30° the beam of the radiometer was never directed at or above the horizon. Such brightness temperature differences were observed during banking over many of the other areas; desert, jungle, farmland, etc. Figure 16 shows the variation of brightness temperature as a function of the scanning angle over the Arctic Ocean ice cap approximately 100 miles north of Point Barrow at 00:41:42 GMT on 31 May.

V. CONCLUSIONS

The Electrically Scanning Microwave Radiometer is capable of producing meteorologically useful and accurate measurements of brightness temperatures within an angle of ±50° from the antenna normal with a beam resolution of about 2.7°. Scan rates can be matched to the speed and height of the carrier vehicle so that contiguous radiation maps can be obtained from aircraft flying above about 3 km and from spacecraft.

Preliminary results from about 75 hours of aircraft flights over a multitude of large scale terrain, cloud and ice formations, and over water, indicate that this instrument is very well suited for: the identification and mapping of cloud formations containing precipitation; for mapping contrasts between water, land and ice; for the detection and mapping of water even under a snow or ice surface; for estimating the thickness of ice; for mapping earth surface temperatures of vegetated regions and for mapping the contrasts between various degrees of vegetation. Radiation measurements at this wavelength are practically unaffected by atmospheric conditions and cloudiness except for clouds containing substantial amounts of precipitation.

We are hopeful that quantitative analysis of the brightness temperatures will yield more definitive results regarding the derivations of precise amounts of precipitation, soil moisture, ice thickness and degree of vegetation from the emissivities measured with this instrument at a wavelength of 1.55 cm.

ACKNOWLEDGEMENT

We are indebted to Mrs. Barbara Sparkman for making available to us measurements of emitted radiation at wavelengths between 10.6 and 11.6 microns in the infrared. These were obtained simultaneously with the microwave observations and have been extremely useful in assessing the performance of the microwave radiometer.

REFERENCES

1. Final Engineering Report on Meteorological Microwave Radiometer, under NASA Contract NAS5-9680 to Space General Corporation, El Monte, California dated July 1967, SGC 939 R - B.

2. Proposal "A Microwave Radiometer for the Nimbus D Meteorological Satellite", Patrick Thaddeus, Goddard Institute for Space Studies, New York, August 2, 1966.

3. Beuttner, J. K., "Regenortung Von Wettersatelliten Mit Hilfe Von Centimeter Wellen", Naturwissenschaften, 50, 1963, 591 - 592.

4. Private Communication from Mr. R. Ketchum, Naval Oceanographic Office, Washington, D. C.

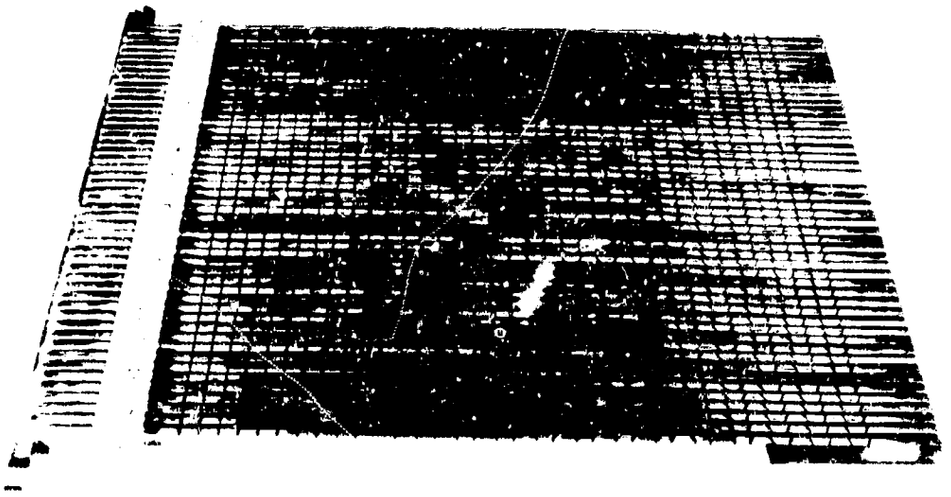

(a) Microwave Antenna

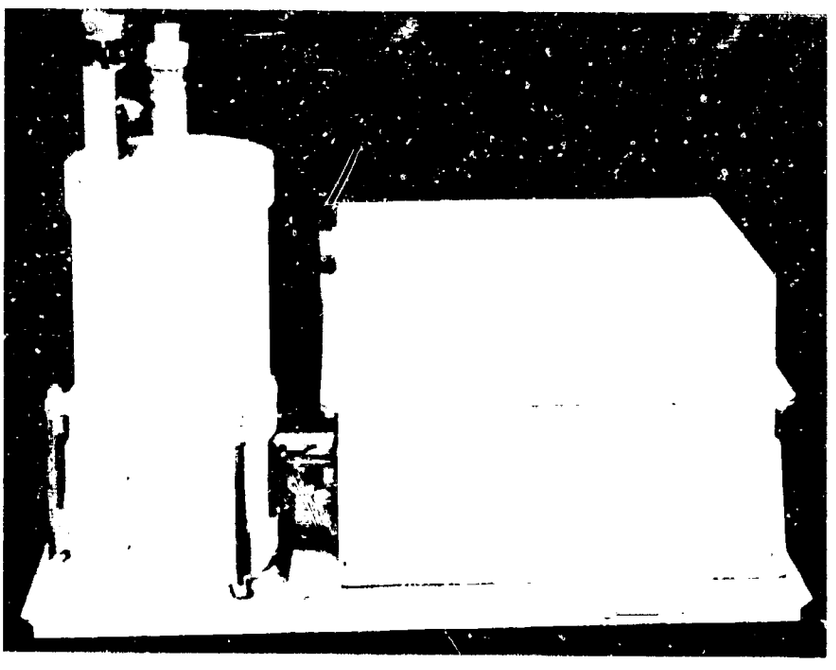

(b) Microwave Receiver with Nitrogen Dewar

Figure 1. Microwave Radiometer (a) Antenna; (b) Microwave Receiver with Cryogenic Dewar

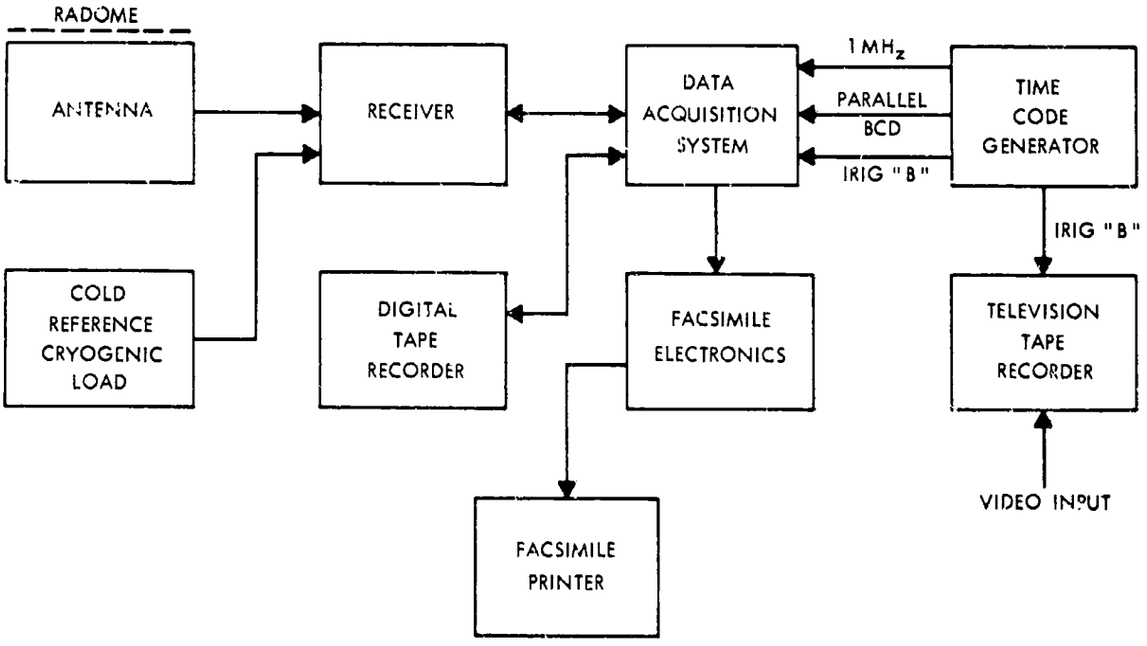

Figure 2. Diagram of Microwave Installation on Aircraft

Figure 3a. Cumulus Cloud over Gulf of Mexico Southeast of New Orleans, Louisiana, Photographed from about 30,000 feet on 6 June 1967.

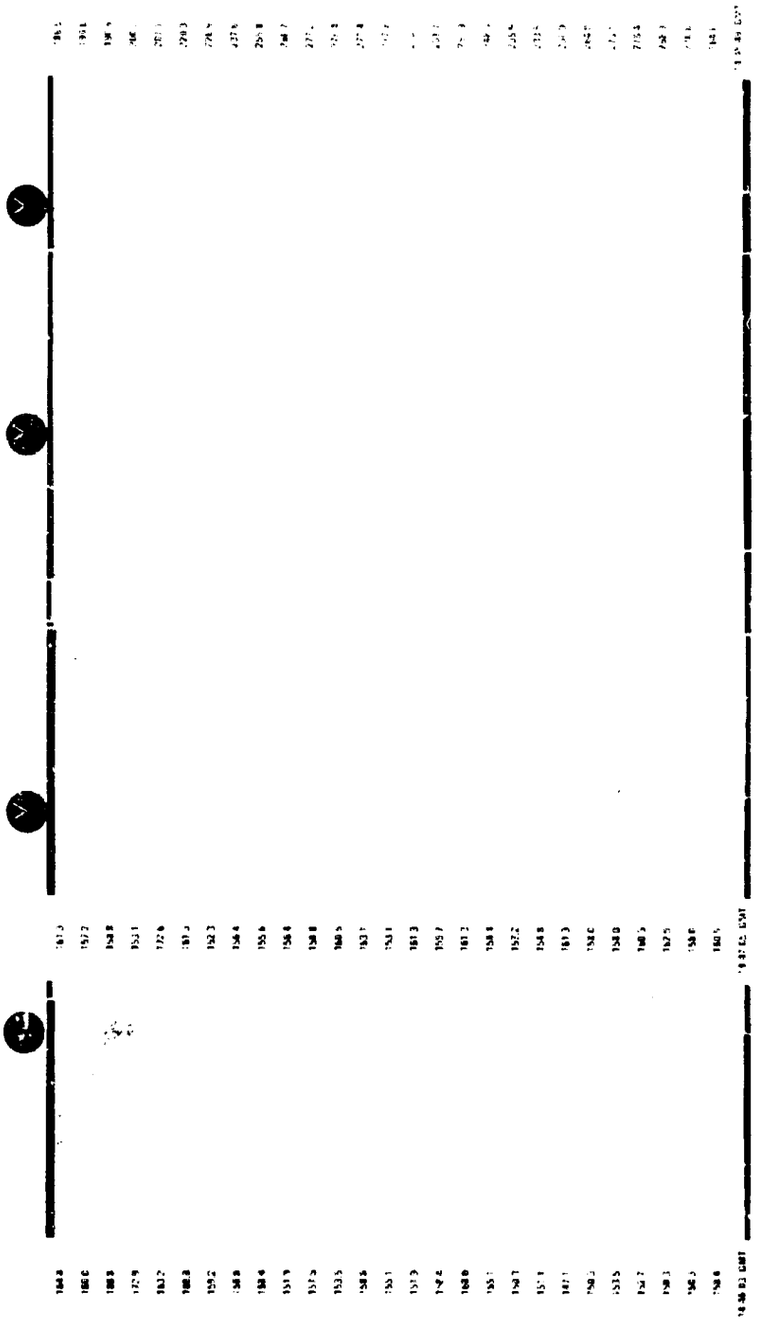

Figure 3b. Cumulo nimbus Cloud over Gulf of Mexico, Southeast of New Orleans, Louisiana, Photographed from about 36,000 feet on 6 June 1967.

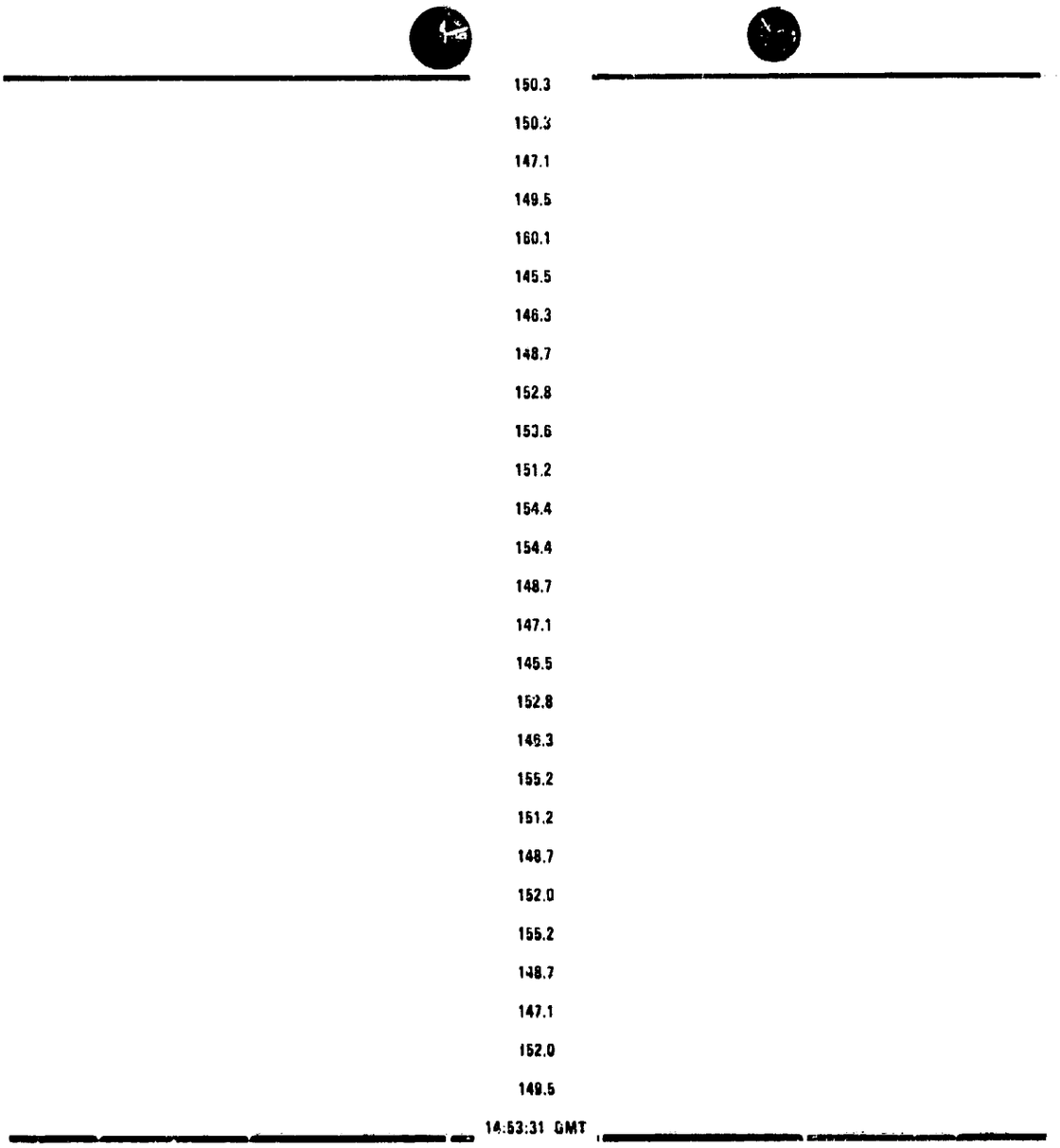

Figure 3c. Cirrus Cloud over Gulf of Mexico, Southeast of New Orleans, Louisiana, Photographed from about 38,000 feet on 6 June 1967.

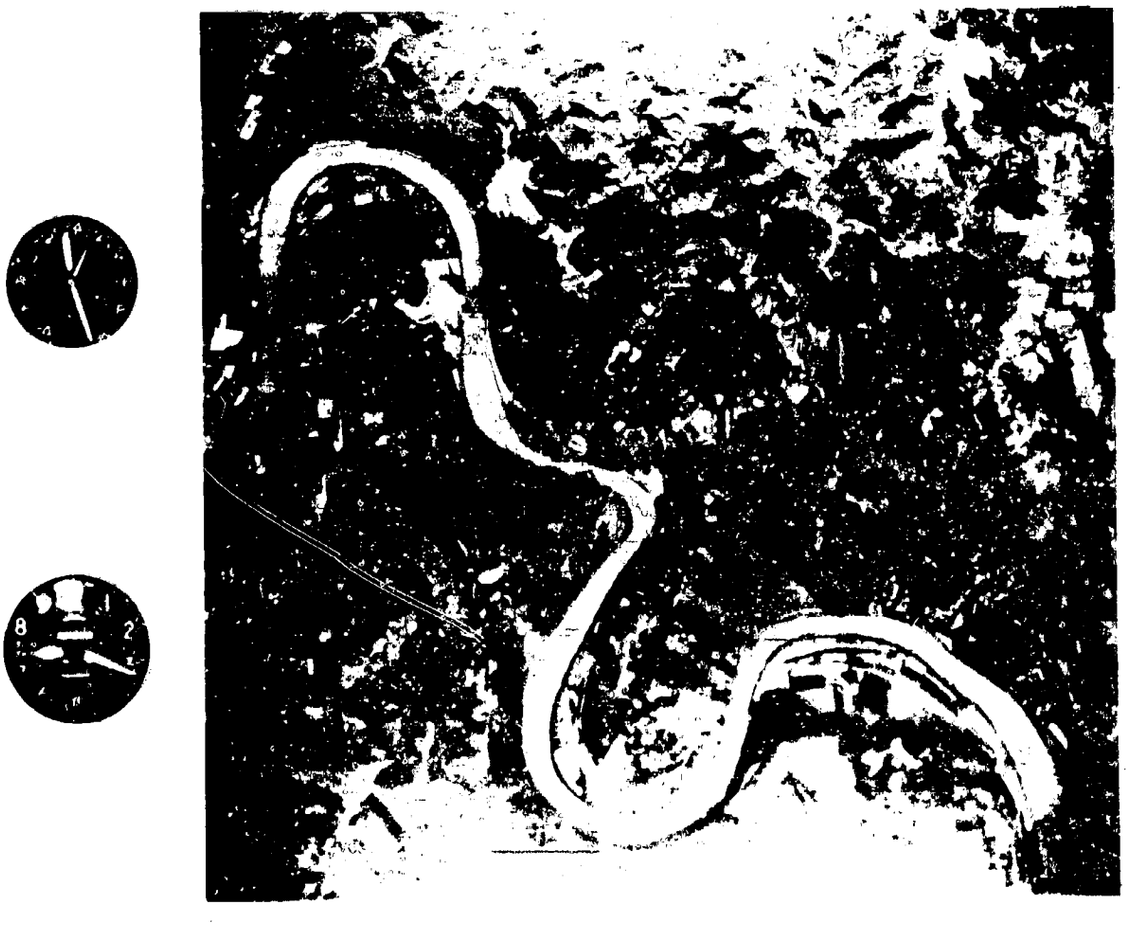

Figure 4a. A Facsimile Display of Brightness Temperatures over Ohio River 37 Miles West of Louisville, Kentucky on 11 May 1967.
Figure 4b. Aerial Photograph of Section of Region Corresponding to Figure 4a.

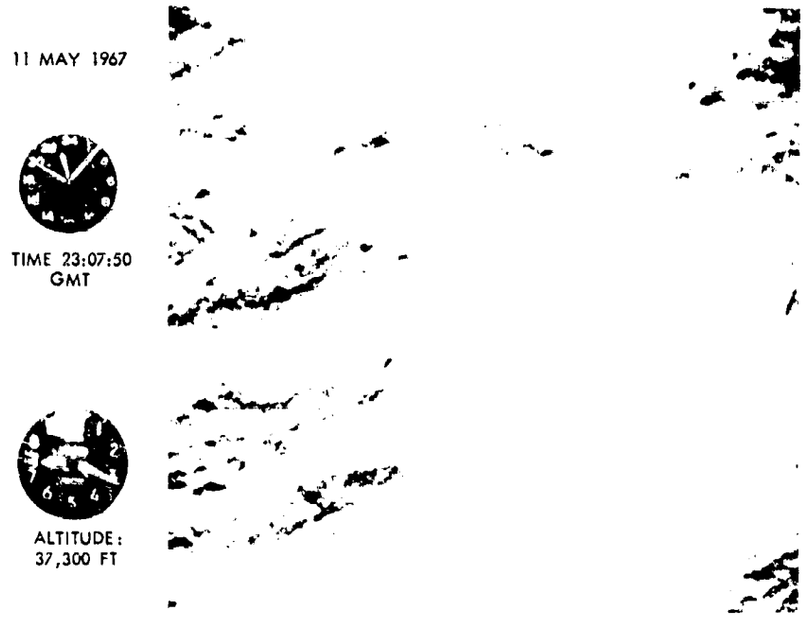

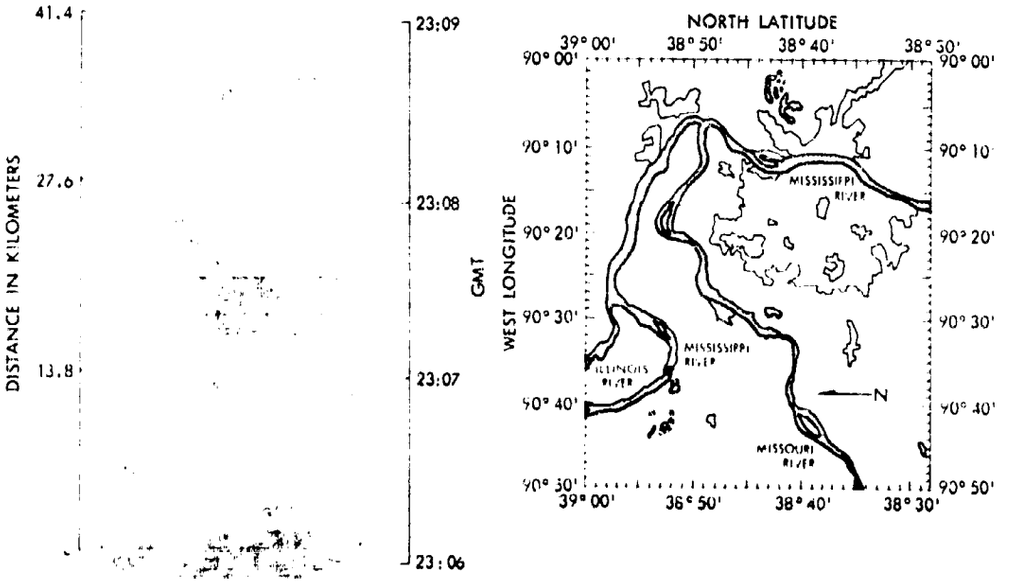

Figure 5a. Aerial Photograph of Cloud Cover over St. Louis, Missouri, on 11 May 1967.
Figure 5b. Facsimile Display of Brightness Temperatures Over St. Louis, Missouri, Corresponding to Figure 5a.
Figure 5c. Topographic Map of St. Louis Area.

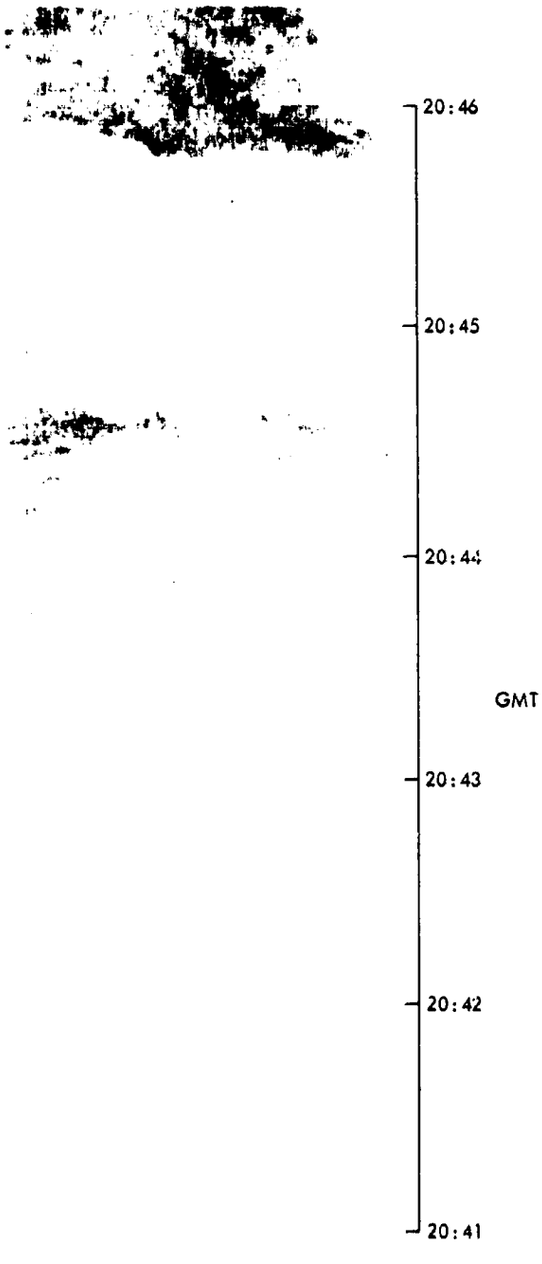

Figure 6a. Facsimile Display of Brightness Temperatures over Sierra Nevada Mountains and Mono Lake on 11 May 1967. Abrupt changes in gray shade are due to manual adjustments of contrast by the operator and should be ignored.

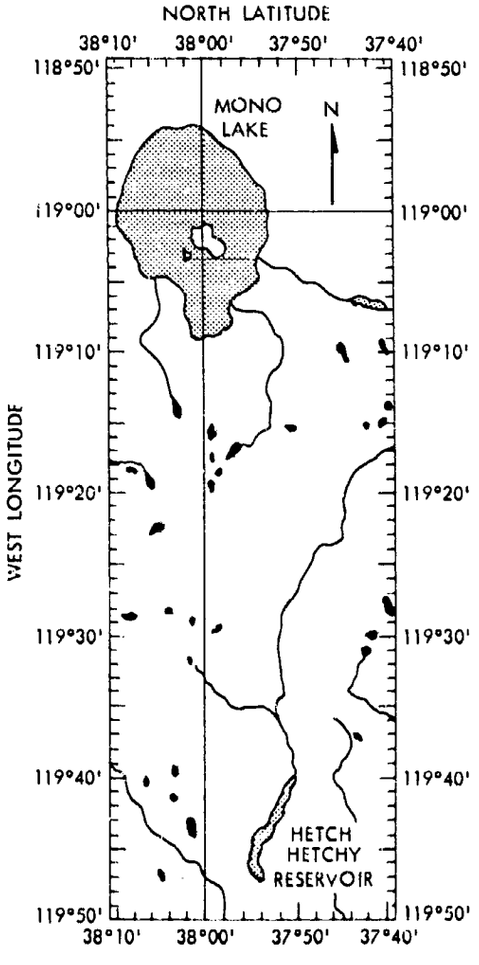

Figure 6b. Topographic Map of Sierra Nevada Mountains and Mono Lake

PRECEDING PAGE BLANK NOT FILMED.

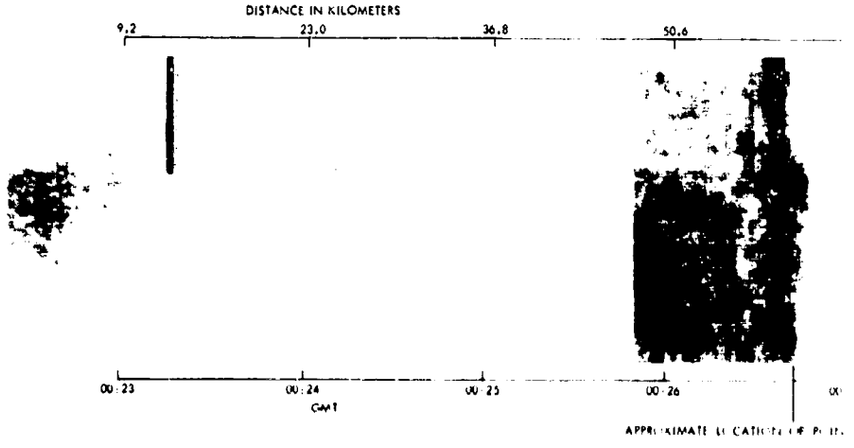

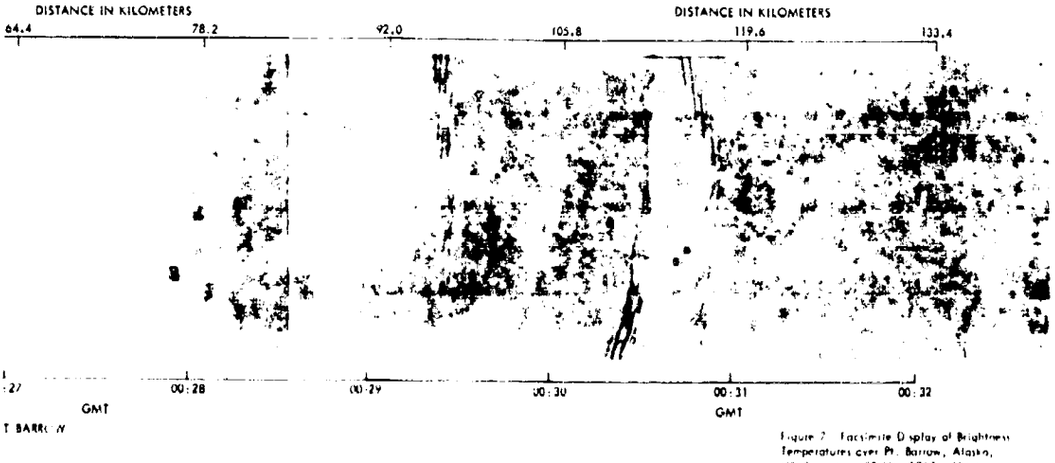

Figure 2. Facsimile Display of Brightness Temperatures over Pt. Barrow, Alaska, (Outbound) on 10 May 1967. Abrupt changes in gray shade are due to manual adjustments of contrast by the operator and should be ignored.

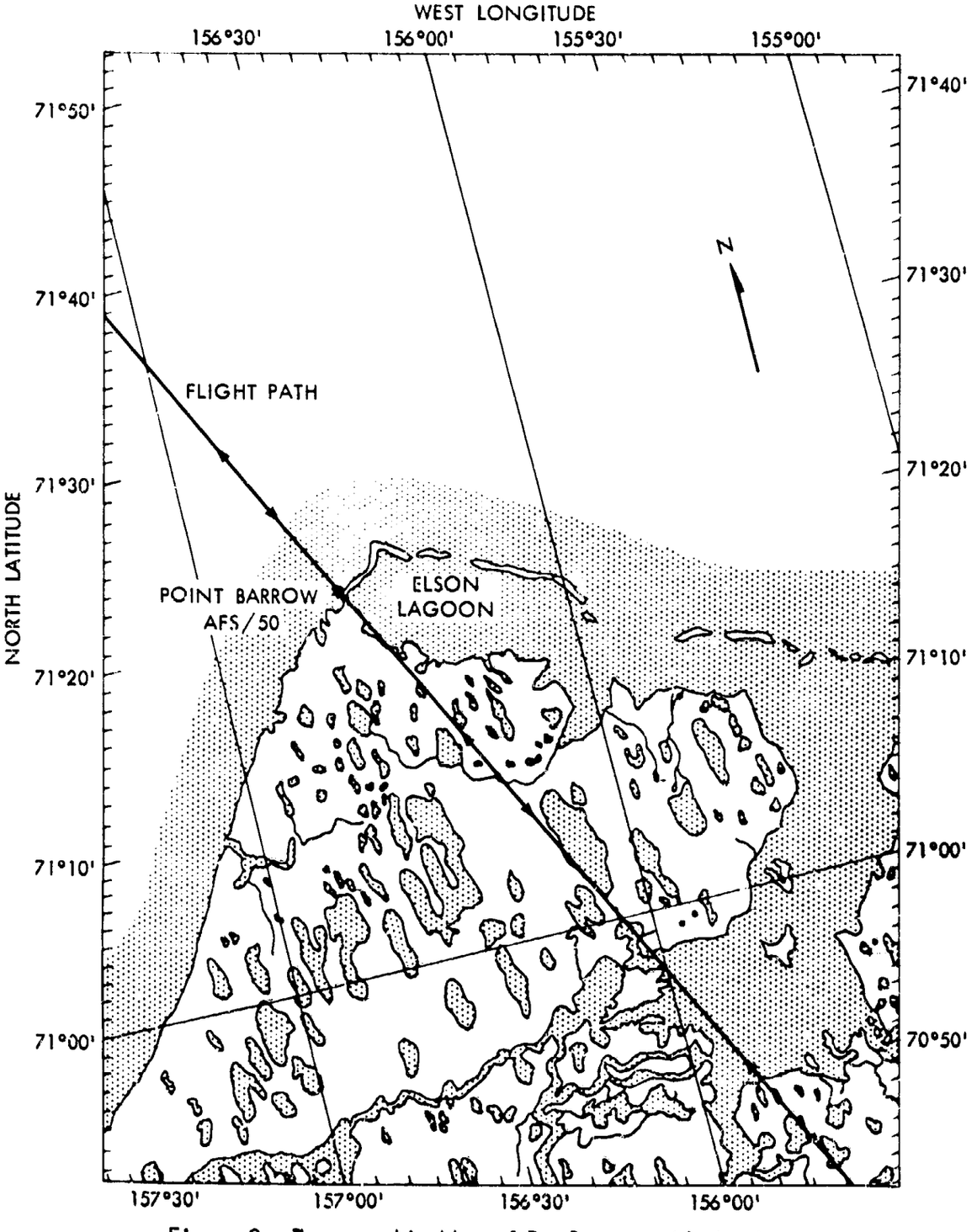

Figure 8. Topographic Map of Pt. Barrow, Alaska Area.

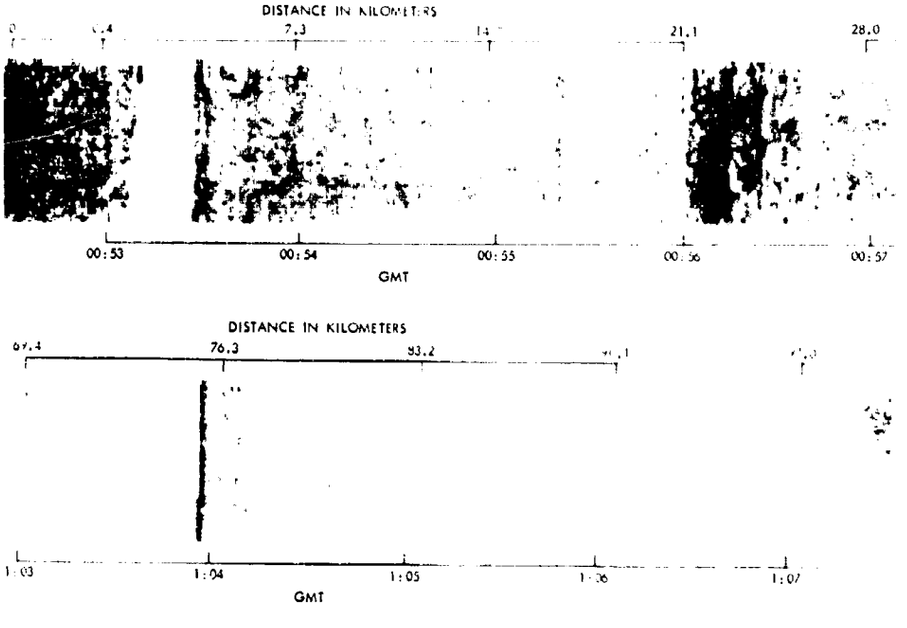
DISTANCE IN KILOMETERS
0
7.3
14
21.1
28.0
00:53
00:54
00:55
00:56
00:57
GMT
DISTANCE IN KILOMETERS
76.3
93.2
1:03
1:04
1:05
1:06
1:07
GMT

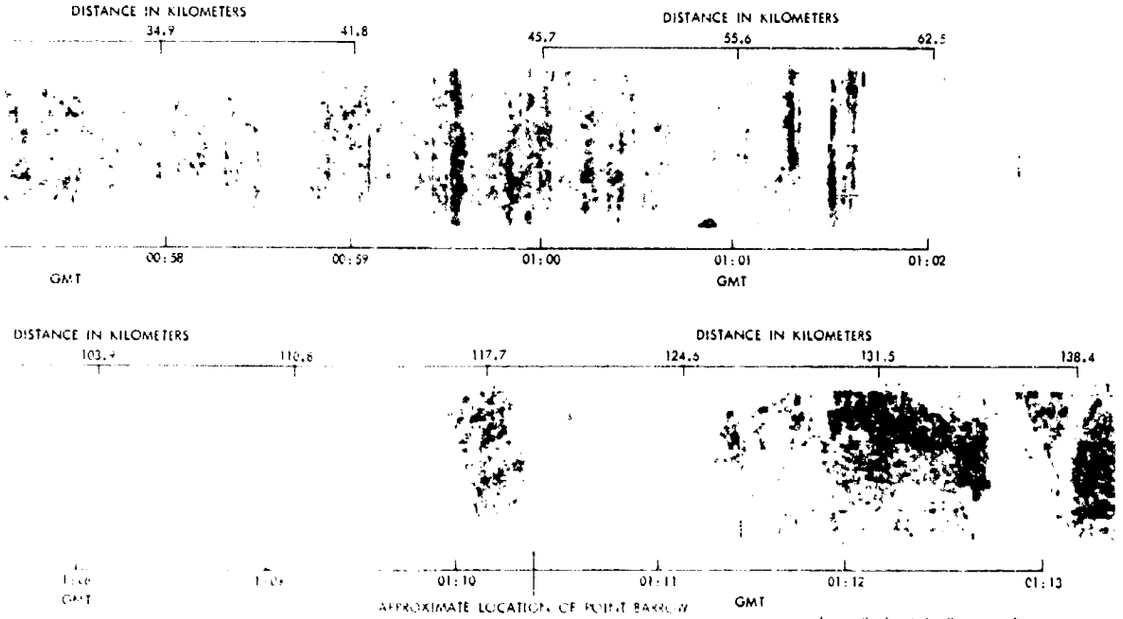
DISTANCE IN KILOMETERS
34.9
41.8
45.7
55.6
62.5
DISTANCE IN KILOMETERS
00:58
00:59
01:00
01:01
01:02
GMT
GMT
DISTANCE IN KILOMETERS
103.9
110.8
117.7
124.6
131.5
138.4
DISTANCE IN KILOMETERS
01:10
01:11
01:12
01:13
GMT
APPROXIMATE LOCATION OF POINT BARROW

Figure 10. Aerial Photograph of Broken Ice off Pt. Barrow on 31 May 1967.

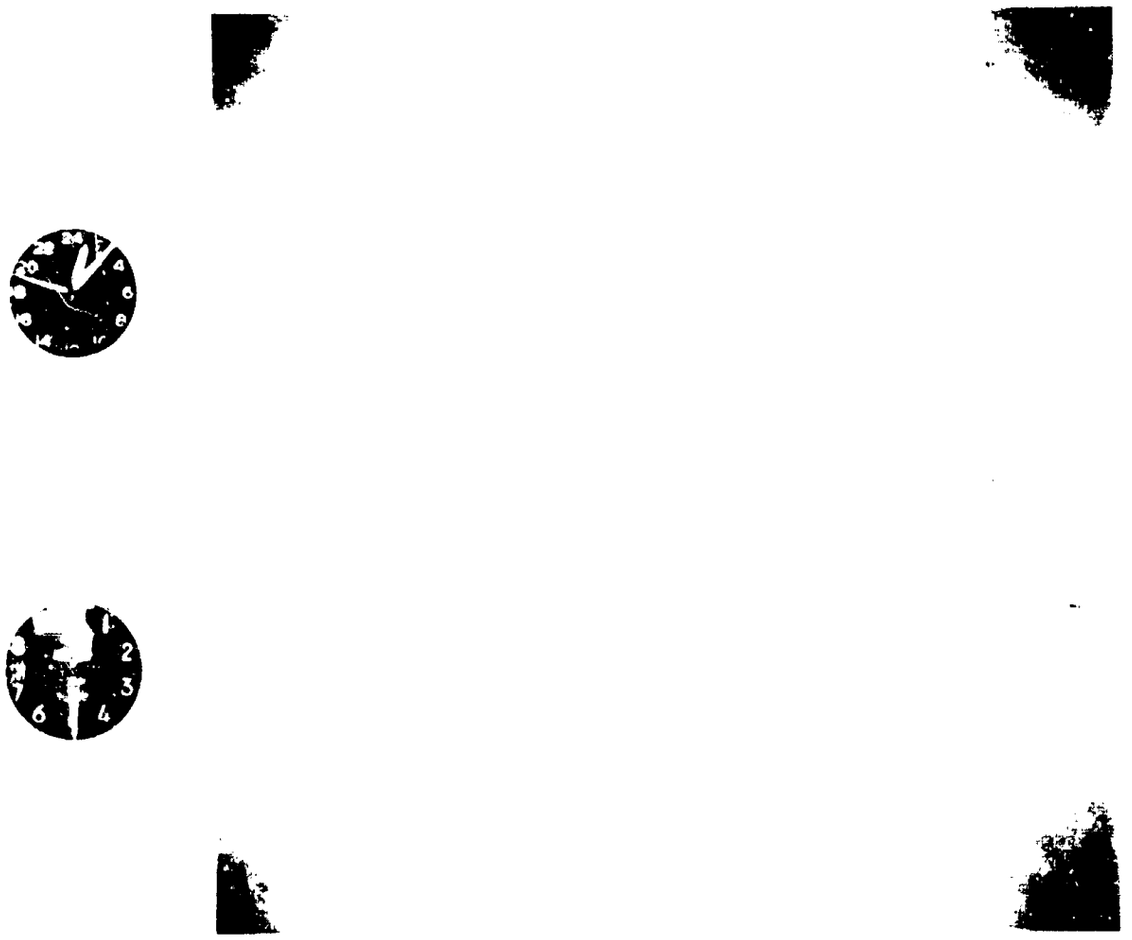

Figure 11. Aerial Photograph of Uniform Snow Fields of Pt. Barrow on 30 May 1967

Figure 12. Aerial Photograph of Lakes and Tundra South of Pt. Barrow on 30 May 1967

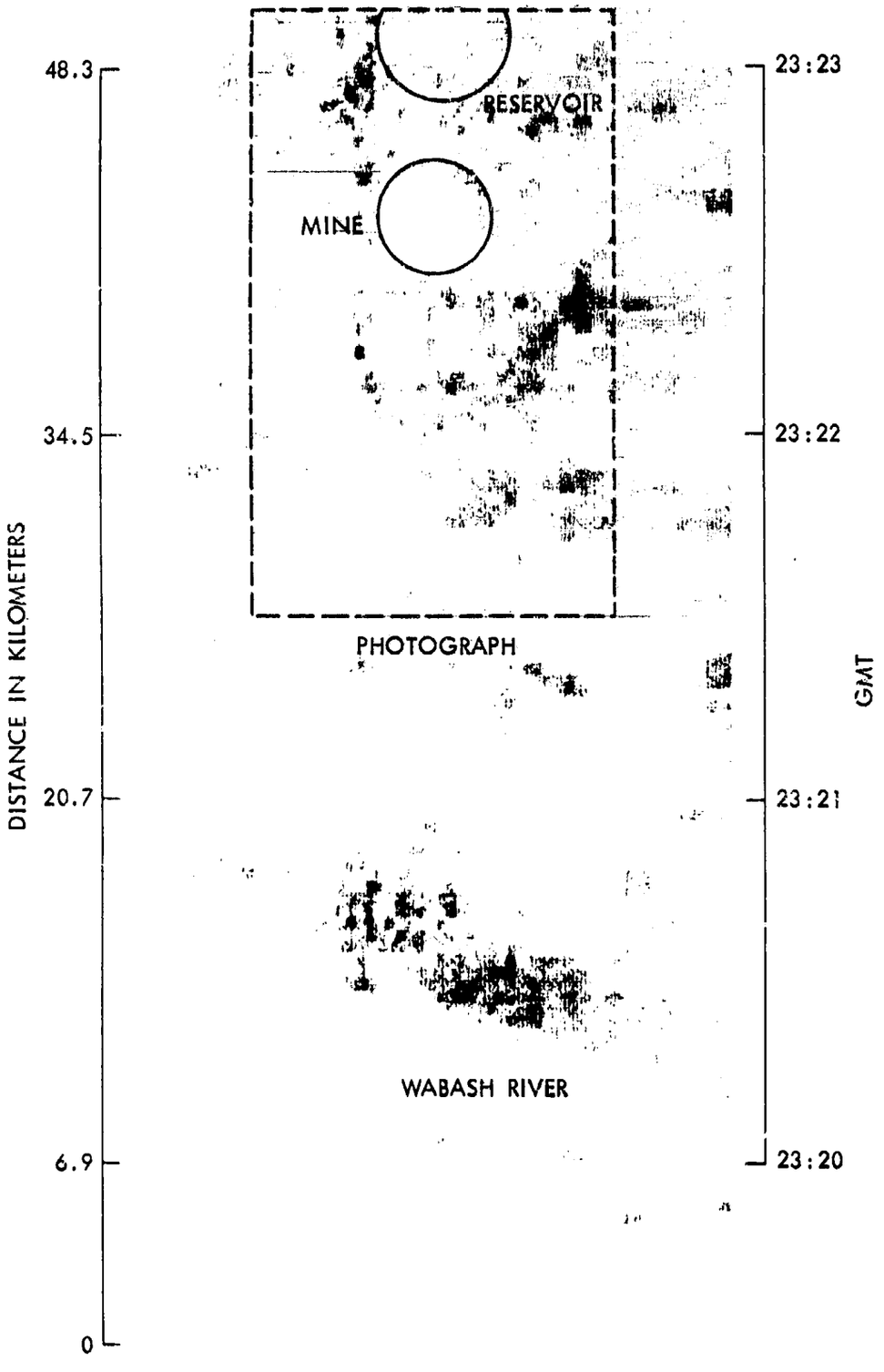

Figure 13. Facsimile Display of Brightness Temperatures over Farmlands near Evansville, Indiana on 11 May 1967.

Figure 14. Aerial Photograph of Farmlands near Evansville, Indiana Corresponding to Figure 13.

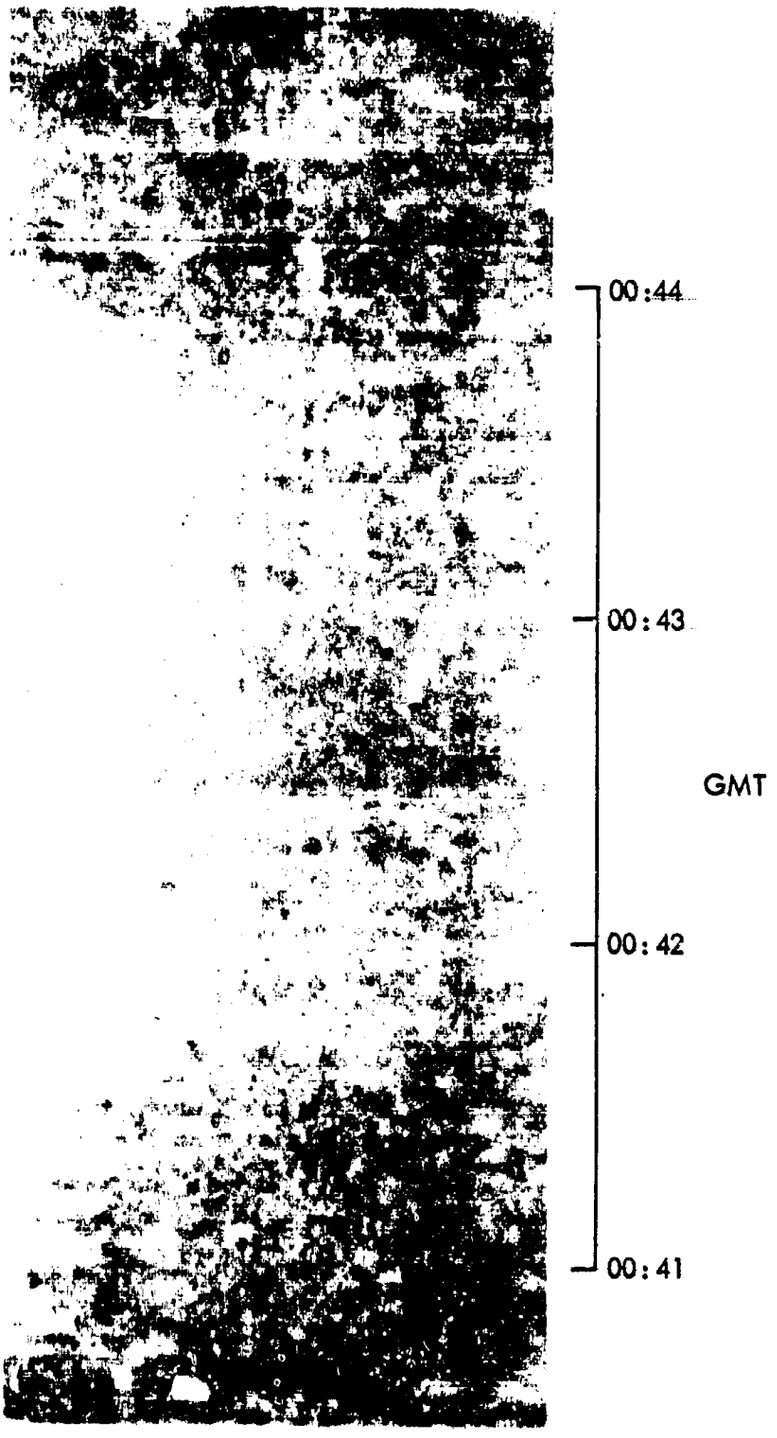

Figure 15. Example of Display of Brightness Temperatures during Aircraft Banking Maneuver over Arctic Ocean Pack Ice North of Pt. Barrow Alaska on 30 May 1967.

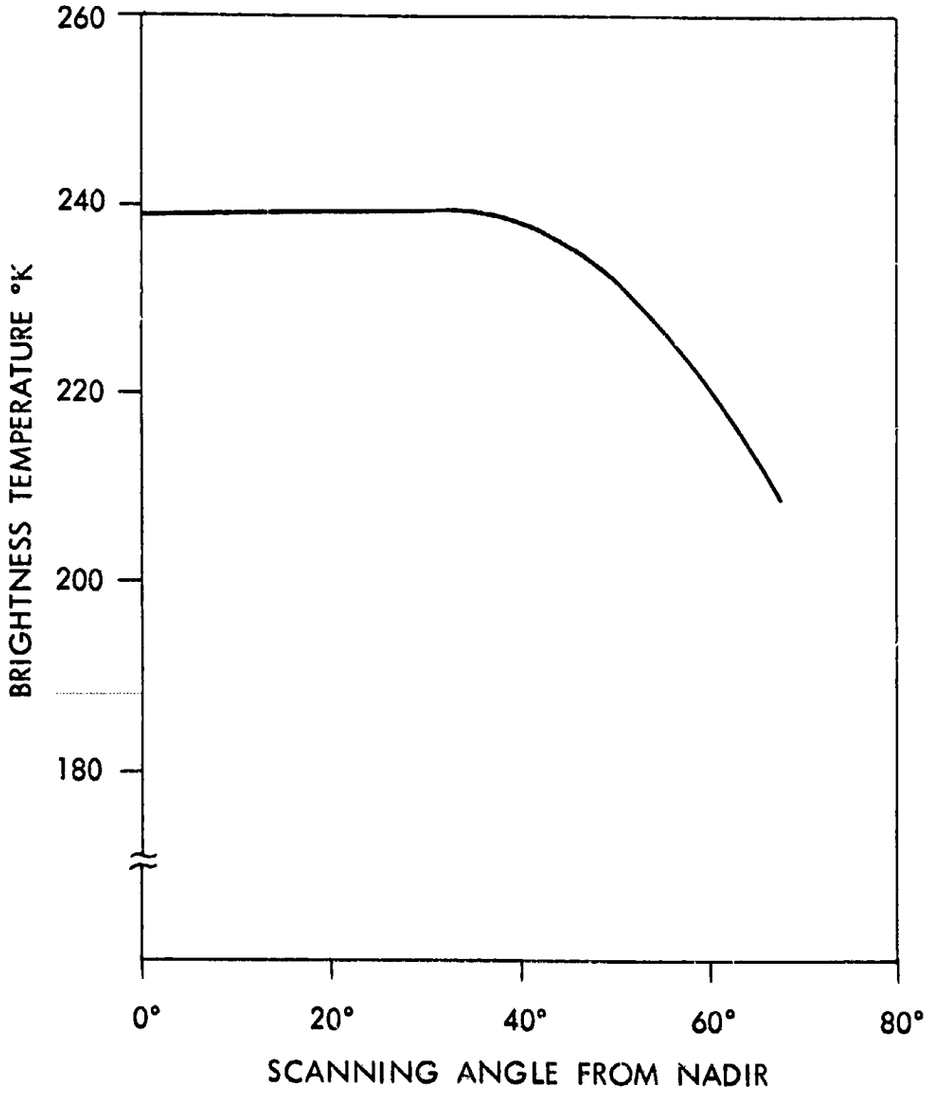

Figure 16. Brightness Temperature vs Scanning Angle at 00:41:42 GMT on 30 May 1967.